

Learning Straight Flows: Variational Flow Matching for Efficient Generation

Chenrui Ma¹ Xi Xiao² Tianyang Wang² Xiao Wang³ Yanning Shen^{1*}

¹University of California, Irvine, Irvine, CA 92697, USA

²University of Alabama at Birmingham, Birmingham, AL 35294, USA

³Oak Ridge National Laboratory, Oak Ridge, TN 37830, USA

Abstract

Flow Matching has limited ability in achieving one-step generation due to its reliance on learned curved trajectories. Previous studies have attempted to address this limitation by either modifying the coupling distribution to prevent interpolant intersections or introducing consistency and mean-velocity modeling to promote straight trajectory learning. However, these approaches often suffer from discrete approximation errors, training instability, and convergence difficulties. To tackle these issues, in the present work, we propose Straight Variational Flow Matching (S-VFM), which integrates a variational latent code representing the “generation overview” into the Flow Matching framework. S-VFM explicitly enforces trajectory straightness, ideally producing linear generation paths. The proposed method achieves competitive performance across three challenge benchmarks and demonstrates advantages in both training and inference efficiency compared with existing methods.

1. Introduction

The goal of generative modeling is to transform a simple prior distribution into a complex data distribution. Flow Matching [1, 9, 28] pursues this objective by learning a velocity field whose associated ODE transports samples from the source distribution to the target distribution [29]. Although Flow Matching adopts linear interpolants as training trajectories, the generative paths it learns are typically *curved* [13, 43]. This curvature arises because the commonly used independent coupling between the source and target distribution results in many intersecting linear interpolants, forcing the learned velocity field to take an average of incompatible directions [11, 21]. As a result, Flow Matching often requires many ODE integration steps to maintain sample quality, limiting its efficiency [17].

Various methods attempt to alleviate this curvature prob-

lem. Some modify coupling strategies [3, 34, 38, 53] or learn improved coupling distributions, aiming to reduce interpolant intersections [23, 41, 44]. Others, such as Rectified Flows [9, 12, 27, 30, 40, 47, 54], iteratively refine the model in multiple distillation stages so that its trajectories gradually approach straight, optimal-transport paths [2, 45]. Meanwhile, Consistency Models [21, 39, 42, 43] and Mean Velocity Models [11, 13, 52] enforce temporal consistency in the learned dynamics, encouraging trajectories at different time steps to agree. Although these approaches embody different design principles—better couplings, iterative refinement, or self-consistency—they share a common motivation: to learn straight generative trajectories. However, they all inherit a fundamental limitation. **Because the independent coupling inherently produces intersecting interpolants, any method that attempts to learn straight trajectories directly from this training structure faces an intrinsic contradiction** [15, 30]. This misalignment often manifests as training instability, discretization artifacts, or difficulty in converging toward truly straight paths.

In this work, we address this contradiction from a new direction. Rather than enforcing straight trajectories under the independent-coupling structure that inherently causes interpolant intersections, we equip the model with the ability to *disambiguate* these intersections. To this end, we introduce the **Straight Variational Flow Matching** framework, which ❶ leverages a variational latent code [5, 22, 33] to provide a global “generation overview” of each source-target pair, enabling the velocity field to choose the correct direction even when interpolants intersecting. Furthermore, we promote ❷ straight trajectory learning by penalizing the time variation of the velocity field along the generative path. Together, these components yield naturally straighter trajectories that require far fewer ODE steps to simulate while maintaining high generation quality [7, 10].

Extensive experiments demonstrate that the proposed method achieves state-of-the-art performance in generation quality, sampling efficiency, and training stability across multiple benchmark datasets. Our theoretical analysis critically clarifies why existing methods struggle to

*Corresponding author: yannings@uci.edu.

learn straight trajectories under independent couplings, and shows how our formulation resolves this challenge in a principled and effective manner.

In summary, our contributions are as follows.

- We identify and prove the fundamental contradiction between straight-trajectory learning and the independent coupling structure used in Flow Matching and related approaches, presenting a theoretical motivation for the proposed method.
- We introduce a novel framework that overcomes this contradiction by incorporating a global latent code for disambiguating intersecting trajectories and a straightness objective that encourages time-invariant velocity fields.
- Superior experimental results across three challenge benchmarks confirm our theoretical claims and demonstrate substantial improvements in generation fidelity, efficiency, and stability.

2. Related Works

2.1. Rectified Flow and Distillation

To address the issue of curved generation trajectories, Rectified Flow [9, 12, 27, 30, 40, 47, 54] reformulates the flow-matching learning process into multiple iterative stages. Specifically, it first trains a basic flow-matching model, then uses the data pairs generated by this model to train a new one [53]. This process is repeated iteratively. Essentially, each subsequent model refines the quality of the training data pairs—reducing trajectory intersections and curvature—by leveraging the outputs of the previous model [30]. This pipeline is also known as distillation [40]. Through this progressive refinement, the model gradually approaches an optimal transport [24] solution, characterized by straight, non-intersecting trajectories within the generation ODE.

Despite its success in reducing curvature and improving trajectory consistency, Rectified Flows and distillation methods suffer from inefficiency: obtaining the final model requires multiple rounds of training, which are both time- and resource-intensive [36, 46]. Moreover, this iterative process may introduce error accumulation, since each subsequent model is trained on data generated by its predecessor rather than the true data distribution [48]. Consequently, the final distilled model often struggles to surpass the generation fidelity of the initial model trained directly on real data [6, 9]. Plus, these multi-stage and tightly-scheduled procedures suffer from a need to specify when to end training and begin distillation [40, 49]. In contrast, end-to-end methods are efficient, accurate, and can be trained indefinitely to continually improve.

2.2. Consistency Model and Mean Velocity Model

Consistency Models represent an important step in straight flow learning, functioning as standalone generative mod-

els that eliminate the need for explicit distillation procedures [14, 43]. These models enforce consistency constraints between network outputs at different time steps, ensuring that trajectories converge to identical endpoints [21, 31]. Various formulations and training schemes have been proposed to enhance their stability and sample quality [42].

Mean Velocity Models focus on defining and leveraging flow-based properties between temporal states. For instance, Shortcut Models [11] integrate self-consistency losses with flow matching to capture correlations among flows across discrete time intervals, whereas Inductive Moment Matching [55] extends this principle to stochastic interpolants, enforcing consistency of their moments over time. Building on this, Meanflows [13] introduce a new ground-truth field representing the mean velocity and model it by the identity relationship between mean velocity and instantaneous velocity, while Flow Maps [4] is introduced as integrals of flow fields between two time steps, providing a displacement-based characterization complementary to the average-velocity perspective. Together, these methods aim to bridge the gap between local flow dynamics and global consistency in generative processes. Recent studies have sought to unify Consistency Models and Mean Velocity Models, demonstrating that these two classes of methods are mathematically equivalent, differing primarily in their model parameterizations and training procedures [18, 50]. Although both Consistency Models and Mean Velocity Models move toward a fully end-to-end generative paradigm, their heavy reliance on bootstrapping necessitates carefully scheduled training processes [11, 21]. Moreover, these approaches often suffer from discrete approximation errors [14, 43], training instability [43], and convergence challenges [13, 19, 50, 52]. In contrast, the proposed method builds upon the Variational Flow Matching framework [15] with a straightness objective, representing a distinct direction from the methods discussed above.

3. Preliminary

Notation. For a random process $X = \{X_t\}_{t \in [0,1]}$, write $\text{Law}(X_t)$ for its marginal law at time t , and $\mathbb{E}[\cdot]$ for expectation.

3.1. Flow Matching

Let (X_0, X_1) be any coupling on \mathbb{R}^d with joint density $\rho(x_0, x_1) = \rho_0(x_0) \rho_1(x_1)$, where $\rho_0(x_0)$ is source distribution (e.g Gaussian) and $\rho_1(x_1)$ is target data distribution (e.g image samples). Define the linear interpolation and *conditional velocity*:

$$X_t = (1-t)X_0 + tX_1, \quad \Delta^X = X_1 - X_0, \quad t \in [0, 1]. \quad (1)$$

Flow Matching models the generation process as an ordinary differential equation (ODE):

$$\frac{d}{dt}X_t = v^X(X_t, t) \quad \text{for } t \in [0, 1]. \quad (2)$$

The associated *marginal velocity* is

$$v^X(x, t) = \mathbb{E}[\Delta^X | X_t = x], \quad (3)$$

The Flow Matching model parameterized by θ is trained by minimizing the Conditional Flow Matching loss:

$$\mathcal{L}_{\text{FM}}(\theta) = \mathbb{E}\left[\|v_\theta(X_t, t) - \Delta^X\|^2\right], \quad (4)$$

instead of the Marginal Flow Matching loss, which is intractable [28, 29]. Although the linear interpolation path is defined in Eq (1), the learned generating ODE trajectories X are curves, since the *marginal velocity* in Eq (3) equals the conditional expectation of *conditional velocity* Δ^X . These trajectories X are rectifiable as defined below [30].

Definition 1 (Rectifiability of X). We say that X is *rectifiable* if $v^X(\cdot, t)$ is locally bounded for each t and the *continuity equation* [28, 29]:

$$\partial_t \pi_t + \nabla \cdot (v^X(\cdot, t) \pi_t) = 0, \quad \pi_{t=0} = \text{Law}(X_0),$$

admits a unique solution $\{\pi_t\}_{t \in [0, 1]}$. Equivalently, the ordinary differential equation $\dot{X}_t = v^X(X_t, t)$ admits a unique flow of characteristics.

3.2. Interpolants Intersection

Definition 2 (Non-intersection functional). For any coupling (X_0, X_1) with linear interpolant X_t , define

$$V((X_0, X_1)) = \int_0^1 \mathbb{E}\left[\|\Delta^X - \mathbb{E}[\Delta^X | X_t]\|^2\right] dt. \quad (5)$$

Lemma 1 (Non-intersection \equiv zero conditional variance). See the proof in the Appendix. For a coupling (X_0, X_1) with linear interpolation X_t , the following are equivalent:

1. For two independent identically distributed couplings (X_0, X_1) and (X'_0, X'_1) ,
$$\exists t \in (0, 1) : (1-t)X_0 + tX_1 = (1-t)X'_0 + tX'_1$$

$$\mathbb{P}[(X_0, X_1) \neq (X'_0, X'_1)] = 0.$$
2. $V((X_0, X_1)) = 0$; equivalently $\Delta^X = \mathbb{E}[\Delta^X | X_t]$ for $t \in (0, 1)$.

The curved ODE trajectories X learned by Flow Matching arise from the intersection of interpolants, which is undesirable, as it leads to $V((X_0, X_1)) \neq 0$. Consequently, multiple sampling steps are required to simulate the ODE trajectory with a tolerable discretization error:

$$X_{t_{i+1}} = X_{t_i} + (t_{i+1} - t_i) v_\theta(X_{t_i}, t_i) \quad (6)$$

rather than a few-step or even a one-step generation.

4. Method

4.1. Straight Interpolants

Ideally, the generation trajectories are *straight interpolants*, whose specific definition compatible with Flow Matching trajectories X is shown below.

Definition 3 (Straight interpolation compatible with X). A process $Z = \{Z_t\}_{t \in [0, 1]}$ on the same probability space as X is called a *straight interpolants* compatible with Flow Matching trajectories X if the following hold:

- (Z1) **Linear paths.** There exist random endpoints (Z_0, Z_1) with $Z_t = (1-t)Z_0 + tZ_1$ and $\Delta^Z = Z_1 - Z_0$.
- (Z2) **Non-intersection.** $V((Z_0, Z_1)) = 0$. Equivalently, $\Delta^Z = \mathbb{E}[\Delta^Z | Z_t]$ for $t \in [0, 1]$.
- (Z3) **Velocity-field matching.** With $\mu_t = \text{Law}(Z_t)$, for $x \sim \mu_t$ and $t \in [0, 1]$,

$$v^Z(x, t) = \mathbb{E}[\Delta^Z | Z_t = x] = v^X(x, t).$$

- (Z4) **Initialization.** $Z_0 = X_0$.

The *straight interpolants* Z satisfy several key properties as shown below.

Theorem 2 (Marginal preservation). See the proof in the Appendix. Assume X is rectifiable and Z satisfies Definition 3. Then $\text{Law}(Z_t) = \text{Law}(X_t)$ for all $t \in [0, 1]$.

Theorem 3 (Convex transport-cost reduction). See the proof in the Appendix. Under the assumptions of Theorem 2, for any convex $c : \mathbb{R}^d \rightarrow \mathbb{R}$,

$$\mathbb{E}[c(Z_1 - Z_0)] \leq \mathbb{E}[c(X_1 - X_0)].$$

If c is strictly convex, equality holds if and only if $V((X_0, X_1)) = 0$.

Thus, we further conclude the equivalent traits of *straight interpolants* for Flow Matching trajectories.

Theorem 4 (Equivalent characterizations of straight interpolants). See the proof in the Appendix. Assume X is rectifiable and Z satisfies Definition 3. The following are equivalent: when they hold, we say X yielded from couplings (X_0, X_1) are straight interpolants, which coincide with Z .

- (i) **Tight convex cost.** There exists a strictly convex c with $\mathbb{E}[c(Z_1 - Z_0)] = \mathbb{E}[c(X_1 - X_0)]$.
- (ii) **Endpoint coincidence.** $(Z_0, Z_1) = (X_0, X_1)$.
- (iii) **Pathwise equality.** $Z_t = X_t$ for all $t \in [0, 1]$.
- (iv) **Non-intersection for X .** $V((X_0, X_1)) = 0$.

Conclusively, for Flow Matching, the objective of learning straight generation trajectories both implies and is ensured by the condition $V((X_0, X_1)) = 0$. However, this objective is unattainable for Flow Matching because the

learned *marginal velocity* in Eq. (3) is the conditional expectation of the *conditional velocity* Δ^X . As a result, $V((X_0, X_1)) \neq 0$, caused by the intersections of multiple linear interpolations defined in Eq. (1) at X_t under the independent coupling $\rho(x_0, x_1) = \rho_0(x_0) \rho_1(x_1)$.

4.2. Vanishing Time Derivative Along X

To achieve $V((X_0, X_1)) = 0$, we propose to minimize the time derivative of the learned velocity field: $\frac{d}{dt}v$.

Definition 4 (Time derivative). For a differentiable vector field $v : \mathbb{R}^d \times [0, 1] \rightarrow \mathbb{R}^d$, the time derivative along its characteristics is

$$\begin{aligned} \frac{d}{dt}v(x, t) &= D_t v(x, t) := \frac{\partial v}{\partial t} \frac{dt}{dt} + \frac{\partial v}{\partial x} \frac{dx}{dt} \\ &= \frac{\partial}{\partial t}v(x, t) + (\nabla_x v(x, t)) v(x, t) \end{aligned} \quad (7)$$

Theorem 5 (Straightness \equiv vanishing time derivative along X). *See the proof in the Appendix. Assume X is rectifiable and Z satisfies Definition 3. Assume moreover that v^X is continuously differentiable in (x, t) . Then $V((X_0, X_1)) = 0$, if and only if $D_t v^X(X_t, t) = 0$, for $t \in [0, 1]$.*

Nevertheless, directly minimizing $D_t v^X(X_t, t)$ conflicts with the Flow Matching objective in Eq. (3), since the intersections produced by the independent coupling make the marginal velocity fundamentally incompatible with straight-trajectory learning. Existing methods, as reviewed in the Related Works section, ultimately aim for the same condition $V((X_0, X_1)) = 0$, which is equivalent to enforcing $D_t v^X(X_t, t) = 0$. However, because they operate within this inherently contradictory formulation, their effectiveness remains fundamentally limited.

4.3. Variational Flow Matching for Straightness

Instead of these existing methods, we introduce Variational Flow Matching with a straightness objective to enforce vanishing time derivative along trajectories, thereby achieving $V((X_0, X_1)) = 0$.

The generation process of Flow Matching is basically a Markov process [37] that predicts the velocity $v^X(X_{t_i}, t_i)$ at time t_i using the current sample X_{t_i} to obtain the next sample $X_{t_{i+1}}$ at time t_{i+1} , as shown in Eq. (6). This procedure implies that the model lacks awareness of the “generation overview” of the trajectories, which is a key reason why interpolants intersect and the learned ODE trajectories become curved. Variational Flow Matching (VFM) [15], parameterized by θ , incorporates a latent code z obtained via a variational autoencoder (VAE) parameterized by ϕ :

$$\begin{aligned} q_\phi(z|X_0, X_1, X_t, t) &= \\ \mathcal{N}(z; \mu_\phi(X_0, X_1, X_t, t), \sigma_\phi(X_0, X_1, X_t, t)), \end{aligned} \quad (8)$$

which involves the “generation overview” information (X_0, X_1) . To predict the velocity $v(X_t, t, z)$, we minimize:

$$\begin{aligned} \mathcal{L}_{\text{VFM}}(\theta, \phi) &= \mathbb{E} \left[\|v_\theta(X_t, t, z) - \Delta^X\|^2 \right] + \\ &\quad \beta D_{KL}(q_\phi(z|X_0, X_1, X_t, t) \| p(z)), \end{aligned} \quad (9)$$

where KL divergence term prevent the posterior distribution $q_\phi(z|X_0, X_1, X_t, t)$ far from prior $p(z) = \mathcal{N}(z; 0, I)$, and its strength is governed by the hyperparameter β [5].

We do not seek to achieve non-intersection for X as in Theorem 4. Instead, by leveraging the “generation overview” information provided by z , we aim to obtain a flow model $v_\theta(X_t, t, z)$ that can distinguish “where to go” even when interpolants are intersected for X . Furthermore, to achieve $V((X_0, X_1)) = 0$, we minimize $D_t v_\theta(X_t, t, z)$. Note that, since VFM incorporates the latent code z , it can handle trajectory intersections; consequently, Z and X become compatible with each other under independent couplings $\rho(x_0, x_1) = \rho_0(x_0) \rho_1(x_1)$ for VFM. This is a key distinction from Flow Matching. See Figure 1. The straightness objective $D_t v(X_t, t, z)$ extends Definition 4:

$$\begin{aligned} D_t v(X_t, t, z) &= \partial_{X_t} v \cdot \frac{dX_t}{dt} + \partial_t v \cdot \frac{dt}{dt} + \partial_z v \cdot \frac{dz}{dt} \\ &= \partial_{X_t} v \cdot v^X(X_t, t, z) + \partial_t v \cdot 1 + \partial_z v \cdot \frac{dz}{dt} \end{aligned} \quad (10)$$

where $\frac{dX_t}{dt} = v^X(X_t, t, z)$ extending from Eq. (2). Further, calculate $\frac{dz}{dt}$ in the same way:

$$\begin{aligned} \frac{dz}{dt} &= \partial_{X_0} z \cdot \frac{dX_0}{dt} + \partial_{X_1} z \cdot \frac{dX_1}{dt} + \partial_{X_t} z \cdot \frac{dX_t}{dt} + \partial_t z \cdot \frac{dt}{dt} \\ &= \partial_{X_0} z \cdot 0 + \partial_{X_1} z \cdot 0 + \partial_{X_t} z \cdot v^X(X_t, t, z) + \partial_t z \cdot 1 \end{aligned} \quad (11)$$

The time derivative shown in Eq. (10) (11) is given by the Jacobian-vector product (JVP) between the Jacobian matrix of each function and the corresponding tangent vector. For code implementation, modern libraries such as PyTorch provide efficient JVP calculation interfaces. Different from previous studies [13] using `torch.func.jvp`, which perform in forward mode and do not retain the computation graph for backward passes, `torch.autograd.functional.jvp` instead retains the graph, thus suitable for our method. In practice, the velocity field $v(X_t, t, z)$ is parameterized as $v_\theta(X_t, t, z)$, and we follow [28] to replace the marginal velocity $v^X(X_t, t, z)$ with the conditional velocity Δ^X . Combining with Eq. (10) (11), the straightness objective is achieved by minimizing:

$$\mathcal{L}_S(\theta, \phi) = \left[\|\partial_{X_t} v \cdot \Delta^X + \partial_t v + \partial_z v \cdot (\partial_{X_t} z \cdot \Delta^X + \partial_t z)\|^2 \right] \quad (12)$$

Thus, the total loss function is formed by Eq. (9) (12):

$$\mathcal{L}(\theta, \phi) = \mathcal{L}_{\text{VFM}}(\theta, \phi) + \alpha \mathcal{L}_S(\theta, \phi) \quad (13)$$

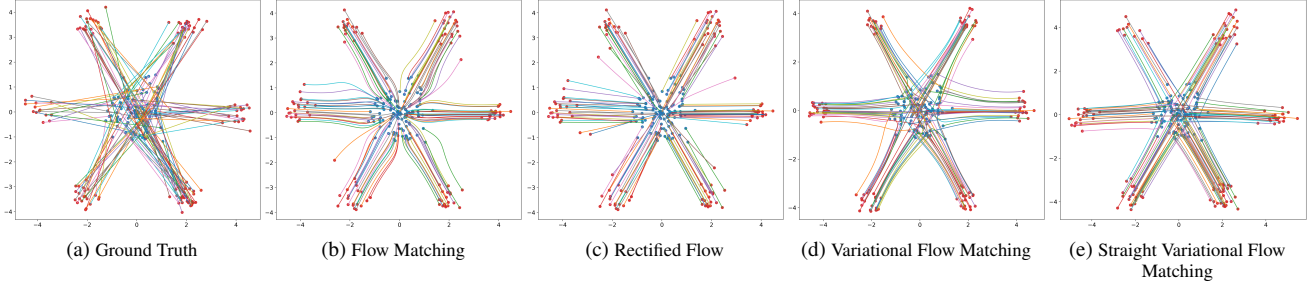


Figure 1. Generation Trajectory Visualization in the 2D Synthesized Hexagonal Dataset.

where the hyperparameter α controls the relative strength of the two components of the loss. See the hyperparameter α, β analysis in the Experiment section. Here, the straightness objective is incorporated into the VFM objective to learn straight generation trajectories, and the latent code z captures the “generation overview”.

In the inference stage, a single latent code z sampled from the prior $p(z)$ is used throughout the generation process from time $t = 0$ to $t = 1$, akin to Eq. (6):

$$X_{t_{i+1}} = X_{t_i} + (t_{i+1} - t_i) v_\theta(X_{t_i}, t_i, z) \quad (14)$$

Since straight trajectories are learned, fewer simulation steps are required compared with Flow Matching in Eq. (6).

5. Experiment

5.1. Synthetic Data

Synthetic data experiments are conducted to visualize the results and intuitively demonstrate the effectiveness of the proposed method. First, we simulate and visualize the generation trajectories of different methods on a 2D hexagonal dataset, as shown in Figure 1. In this dataset, the source distribution (blue points) is a simple Gaussian, while the target distribution (red points) consists of six Gaussian clusters arranged around the source. The visualization results are consistent with the discussion in the previous section: our goal is to learn a straight flow even when the trajectories intersect, which is achieved thanks to the introduction of the VFM framework and straightness objective. Furthermore, we conduct experiments on a more complex synthetic dataset, as illustrated in Figure 2. In this case, the source distribution (blue points) consists of eight Gaussian clusters surrounding the target distribution (red points), which forms an upper-lower moon shape. These results further demonstrate the robustness and generalization capability of our method in modeling complex nonlinear transformations.

5.2. CIFAR-10

CIFAR-10 is a 32×32 resolution image dataset containing multiple classes, and is a widely used benchmark in prior work [25]. For a fair evaluation, we use the same architecture and training paradigm of previous studies [14, 15],

but train the UNet model with the VFM framework with the straightness objective, as shown in Eq. (13).

The UNet v_θ consists of downsampling and upsampling residual blocks with skip connections, and a self-attention block added after the residual block at 16×16 resolution and in the middle bottleneck layer. The model takes both X_t , t and z as input, with the time embedding t used to regress learnable scale and shift parameters for adaptive group norm layers.

The posterior model q_ϕ shares a similar encoder structure as v_θ : image space inputs $[X_0, X_1, X_t]$ are concatenated along the channel dimension, while time t is conditioned using adaptive group normalization. The network predicts μ_ϕ and σ_ϕ with dimensions 768. During training, the variational latent z is sampled from the predicted posterior q_ϕ , and at test time, from a standard Gaussian prior $p(z)$. The latent is processed through two MLP layers and serves as a conditional signal for the velocity network v_θ . We identify two effective approaches as conditioning mechanisms: *adaptive normalization*, where z is added to the time embedding before computing shift and offset parameters, and *bottleneck sum*, which fuses the latent with intermediate activations at the lowest resolution using a weighted sum before upsampling.

Figure 3 illustrates the generation results under different numbers of function evaluations (NFE), using two distinct initial noise sets, X_0^1 and X_0^2 , along with their corresponding latent code sets, z^1 and z^2 , respectively. Note that the noise samples and latent codes within each set are randomly generated following their prior distributions, as described in the Method section, and are independently sampled. Within each row, images at the same grid position across panels are generated from the same initial noise (belonging to X_0^1 or X_0^2) and the corresponding latent code (from z^1 or z^2). Each image panel in a row varies by the number of function evaluations, with NFE values of $[1, 2, 5, 10]$ from left to right. As the NFE increases, both the visual fidelity and structural consistency of the generated images improve. Notably, even the one-step generation (NFE = 1) demonstrates competitive quality compared to multi-step generations, which is a key observation supporting the claim that the proposed method yields *nearly straight generation tra-*

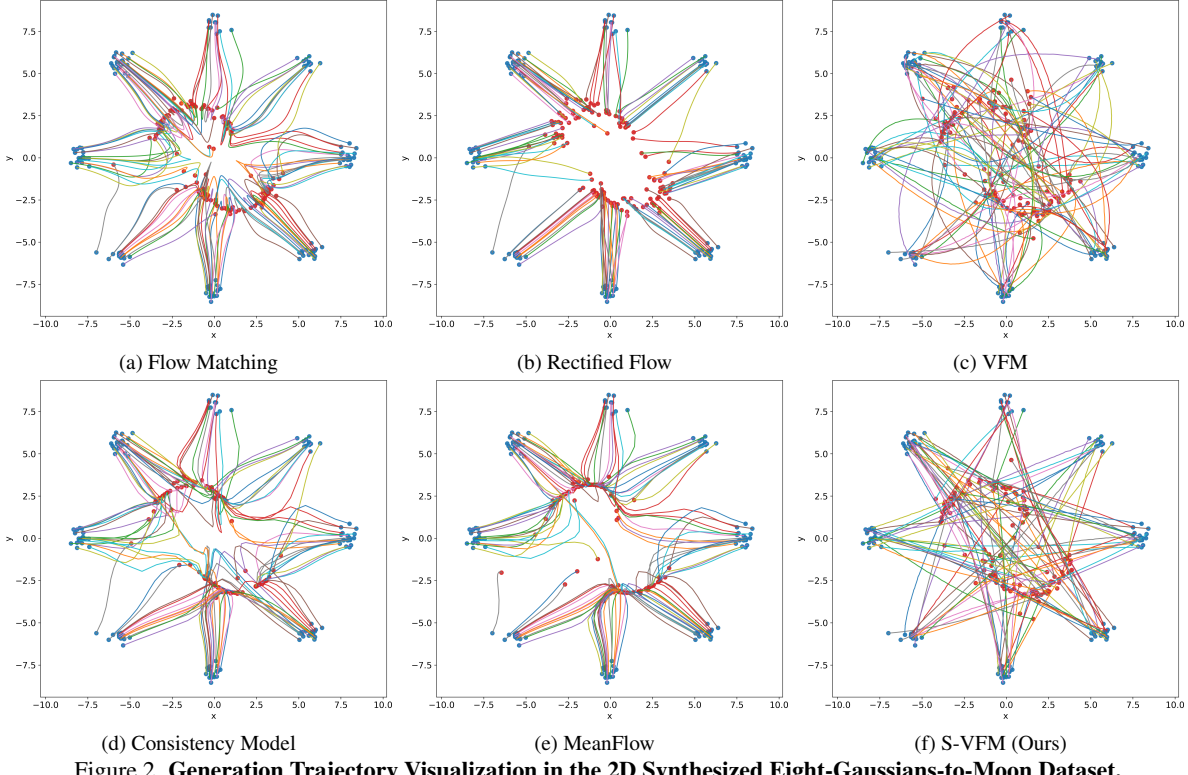


Figure 2. Generation Trajectory Visualization in the 2D Synthesized Eight-Gaussians-to-Moon Dataset.

jectories to support few-steps generation.

Figure 3 also demonstrates the effect of generation from the same latent code under various initial noises: each image panel contains samples generated from different initial noises while keeping the latent code fixed. Furthermore, to investigate the generative behavior under the same initial noise but different latent codes, we visualize two groups of images in Figure 4. Images at the same grid position in panels (a) and (b) are generated from the same initial noise belonging to the noise set X_0^1 , but with different corresponding latent codes from the latent code sets z^1 and z^2 , respectively. The same configuration applies to panels (c) and (d), which differ by the initial noise set X_0^2 and latent code sets z^3 and z^4 . As in the previous experiment, the noise samples and latent codes within each set are randomly drawn from their respective prior distributions, as described in the Method section, and are independently sampled. For all panels, the number of function evaluations is fixed at NFE = 1. The results shown in Figure 4 indicate that images generated from the same initial noise but conditioned on different latent codes exhibit consistent color patterns and similar spatial layouts. However, variations in the latent codes can lead to changes in object class or the presence of different instances of the same class.

To quantitatively evaluate the generation performance, we compare our method with several state-of-the-art approaches by measuring the generation quality using the

Fréchet Inception Distance (FID) [16], computed under varying NFE: [1, 2, 5, 10] and adaptive-step Dopr5 ODE solver [8], as presented in Table 1. Two model variants employing different latent code conditioning mechanisms—*adaptive normalization* and *bottleneck sum*—were tested, with the straightness loss weight fixed at $\alpha = 10$ and the KL loss weight at $\beta = 1e-2$. See the hyperparameter analysis in the Ablation Study section for further details. The results in Table 1 show that our method (*adaptive normalization* variant) achieves the best performance in one-step generation (NFE = 1). Moreover, the FID score consistently decreases as NFE increases, while both Consistency Models and Mean Velocity Models tend to exhibit degraded performance with higher NFE values.

5.3. ImageNet

To evaluate robustness and efficiency on large-scale data, we evaluate methods on the ImageNet 256×256 dataset [26]. For a fair comparison, we use the SiT-XL [35] architecture, a transformer-based model that has shown strong results in image generation, and has been selected as backbone for many previous studies [20, 32, 51]. For a fair comparison, we strictly follow the original training recipe in the open-source SiT repository and replicate the training process from the SiT paper, while introducing our model, S-VFM-XL, by substituting the classic flow matching loss with the straight VFM loss in Equation (13). The

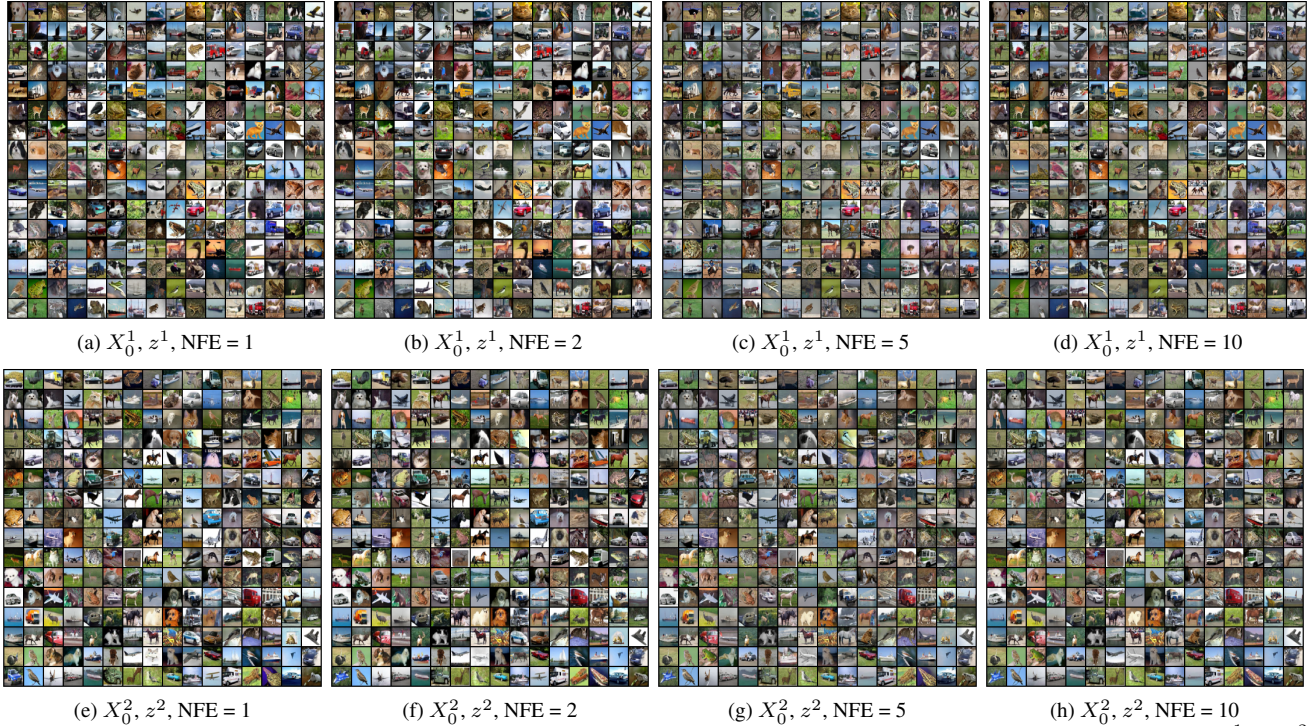


Figure 3. **Randomly Selected Generation Results under Different NFE.** Each row corresponds to a distinct initial noise set (X_0^1 or X_0^2) and its associated latent code set (z^1 or z^2). Within each row, images at the same grid position across panels are generated from the same initial noise and latent code, while panels from left to right correspond to increasing NFE values of $[1, 2, 5, 10]$. Both the noise samples and latent codes are independently drawn from their prior distributions.

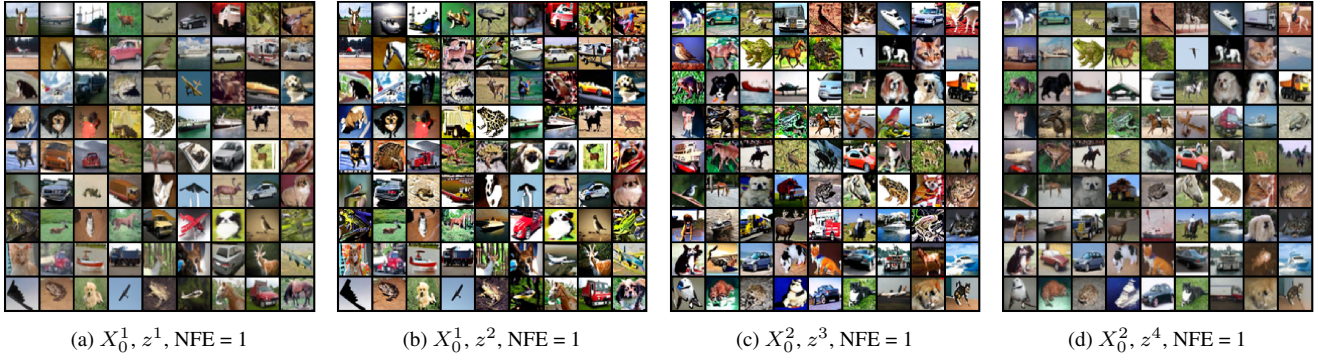


Figure 4. **Generation results under the same initial noise but different latent codes.** Panels (a) and (b) are generated from the same initial noise set X_0^1 with different latent code sets z^1 and z^2 , respectively, while panels (c) and (d) use a different initial noise set X_0^2 with corresponding latent code sets z^3 and z^4 . All noise samples and latent codes are independently drawn from their prior distributions, and the number of function evaluations is fixed at NFE = 1.

posterior model q_ϕ also utilizes an SiT transformer architecture but with half the number of blocks. In the final layer, the features are average-pooled and passed through an MLP layer to predict μ_ϕ and σ_ϕ . We sample the latent code z from the posterior q_ϕ during training and from the prior distribution $p(z)$ during inference. This latent code z is then processed by three MLP layers and fused with the velocity network v_θ via adaptive normalization. By default, we use the Euler-Maruyama sampler with the SDE solver

in the inference stage, as described by SiT [35]. Following the evaluation protocol of previous studies [13, 42], we randomly generate 50K images from each model and report the corresponding FID scores in Table 2. S-VFM-XL consistently outperforms both Consistency Models and Mean Velocity Models, achieving notable gains under identical training conditions. These results highlight the importance of modeling a global *generation overview* within the velocity vector field, which helps resolve ambiguities caused

NFE / Sampler	# Params.	1	2	5	10	Adaptive
Flow	Flow Matching [28] [ICLR'23]	36.5M	-	166.65	36.19	14.4
	VFM [15] [ICML'25]	60.6M	-	97.83	13.12	5.34
Rectified Flow	1-Rectified Flow [30] [ICLR'23]	36.5M	378	6.18	-	-
	2-Rectified Flow [30] [ICLR'23]	36.5M	12.21	4.85	-	-
	3-Rectified Flow [30] [ICLR'23]	36.5M	8.15	5.21	-	3.96
Mean Velocity/ Consistency Models	CT [43] [ICML'23]	61.8M	8.71	5.32	11.412	23.948
	iCT [42] [ICLR'24]	55M	2.83	2.46	-	-
	ECT [14] [ICLR'25]	55M	3.60	2.11	-	-
	sCT [31] [ICLR'25]	55M	2.85	2.06	-	-
	IMM [55] [ICML'25]	55M	3.20	1.98	-	-
	MeanFlow [13] [NIPS'25]	55M	2.92	2.23	2.84	2.27
	Ours	S-VFM (bottleneck sum) [Ours]	60.6M	2.94	2.28	2.06
	Ours	S-VFM (adaptive norm) [Ours]	60.6M	2.81	2.16	1.97

Table 1. **Quantitative Comparison with Different Generation Methods on CIFAR-10 Dataset.** Our method (*adaptive normalization* variant) achieves the best performance in one-step generation (NFE = 1). Moreover, the FID score consistently decreases as NFE increases.

Method	# Params.	NFE	FID
iCT-XL/2 [42] [ICLR'24]	675M	1	34.24
Shortcut-XL/2 [11] [ICLR'25]	675M	1	10.60
MeanFlow-XL/2 [13] [NIPS'25]	676M	1	3.43
S-VFM-XL/2 [Ours]	677M	1	3.31
iCT-XL/2 [42] [ICLR'24]	675M	2	20.30
iMM-XL/2 [55] [ICML'25]	675M	1 \times 2	7.77
MeanFlow-XL/2 [13] [NIPS'25]	676M	2	2.93
S-VFM-XL/2 [Ours]	677M	2	2.86

Table 2. **Quantitative Comparison with Different Generation Methods on ImageNet 256 \times 256 Dataset.** Our method achieves the best performance in few-step generation.

by intersecting interpolants and complements the straightness objective, resulting in straighter generation trajectories that enable few-step generation. In addition, we ana-

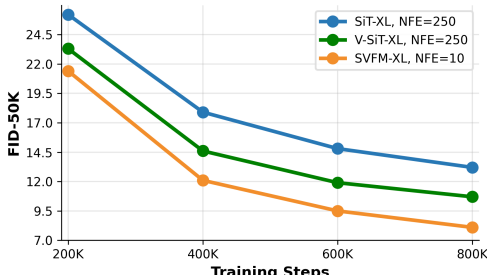


Figure 5. **Comparison of FID-50K Score over Training Iterations on ImageNet 256 \times 256 Dataset.**

lyze model performance across different training iterations, comparing our method with SiT and VFM (S-VFM without the straightness objective), as shown in Figure 5. For SiT and VFM, we follow the default inference setting [15, 35] with NFE = 250, while for the proposed S-VFM, we use NFE = 10 to reflect its few-step generation property. The results demonstrate a consistent performance improvement, further confirming the efficiency and effectiveness of S-VFM in both training and inference.

5.4. Ablation Study

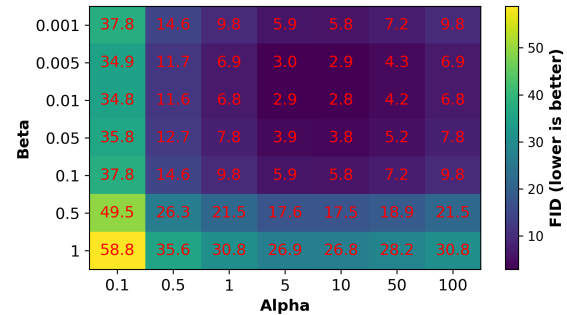


Figure 6. **Ablation Study Results by Adjusting α and β on CIFAR-10 Dataset.** The value in the grid represents the FID score of one-step generation (NFE = 1), lower is better.

To evaluate the contribution of each hyperparameter to S-VFM, we conduct an ablation study by evaluating the generation performance while varying the hyperparameters α and β . Figure 6 presents the one-step generation FID scores for different combinations of α and β on the CIFAR-10 dataset in a heatmap format, where lower values indicate better performance. The results show that S-VFM exhibits a stable performance plateau around the optimal region, suggesting the method is relatively insensitive to hyperparameter variations and demonstrating its adaptive robustness.

6. Conclusion

In this work, we address the key contradiction between straight trajectory learning and the independent coupling implemented in Flow Matching by introducing the Straight Variational Flow Matching framework. By incorporating a variational latent code that offers a global “generation overview,” allowing the model to distinguish between intersecting interpolants. Additionally, by using a straightness objective that penalizes time variations in the velocity field, the model learns to generate naturally straight trajectories.

Acknowledgment

This manuscript was co-authored by Oak Ridge National Laboratory (ORNL), operated by UT-Battelle, LLC under Contract No. DE-AC05-00OR22725 with the U.S. Department of Energy. Any subjective views or opinions expressed in this paper do not necessarily represent those of the U.S. Department of Energy or the United States Government.

References

- [1] Michael Samuel Albergo and Eric Vanden-Eijnden. Building normalizing flows with stochastic interpolants. In *The Eleventh International Conference on Learning Representations*, 2023. 1
- [2] Michael S Albergo, Nicholas M Boffi, and Eric Vanden-Eijnden. Stochastic interpolants: A unifying framework for flows and diffusions, 2023. URL <https://arxiv.org/abs/2303.08797>, 3, 2023. 1
- [3] Michael Samuel Albergo, Mark Goldstein, Nicholas Matthew Boffi, Rajesh Ranganath, and Eric Vanden-Eijnden. Stochastic interpolants with data-dependent couplings. In *International Conference on Machine Learning*, pages 921–937. PMLR, 2024. 1
- [4] Nicholas M Boffi, Michael S Albergo, and Eric Vanden-Eijnden. Flow map matching. *arXiv preprint arXiv:2406.07507*, 2(3):9, 2024. 2
- [5] Christopher P Burgess, Irina Higgins, Arka Pal, Loic Matthey, Nick Watters, Guillaume Desjardins, and Alexander Lerchner. Understanding disentangling in beta-vae. *arXiv preprint arXiv:1804.03599*, 2018. 1, 4
- [6] Shengqu Cai, Eric Ryan Chan, Yunzhi Zhang, Leonidas Guibas, Jiajun Wu, and Gordon Wetzstein. Diffusion self-distillation for zero-shot customized image generation. In *Proceedings of the Computer Vision and Pattern Recognition Conference*, pages 18434–18443, 2025. 2
- [7] Quan Dao, Hao Phung, Trung Tuan Dao, Dimitris N Metaxas, and Anh Tran. Self-corrected flow distillation for consistent one-step and few-step image generation. In *Proceedings of the AAAI Conference on Artificial Intelligence*, pages 2654–2662, 2025. 1
- [8] John R Dormand and Peter J Prince. A family of embedded runge-kutta formulae. *Journal of computational and applied mathematics*, 6(1):19–26, 1980. 6
- [9] Patrick Esser, Sumith Kulal, Andreas Blattmann, Rahim Entezari, Jonas Müller, Harry Saini, Yam Levi, Dominik Lorenz, Axel Sauer, Frederic Boesel, Dustin Podell, Tim Dockhorn, Zion English, and Robin Rombach. Scaling rectified flow transformers for high-resolution image synthesis. In *Forty-first International Conference on Machine Learning*, 2024. 1, 2
- [10] Weilun Feng, Chuanguang Yang, Zhulin An, Libo Huang, Boyu Diao, Fei Wang, and Yongjun Xu. Relational diffusion distillation for efficient image generation. In *Proceedings of the 32nd ACM international conference on multimedia*, pages 205–213, 2024. 1
- [11] Kevin Frans, Danijar Hafner, Sergey Levine, and Pieter Abbeel. One step diffusion via shortcut models. In *The Thirteenth International Conference on Learning Representations*, 2025. 1, 2, 8
- [12] Zhengyang Geng, Ashwini Pokle, and J Zico Kolter. One-step diffusion distillation via deep equilibrium models. In *Thirty-seventh Conference on Neural Information Processing Systems*, 2023. 1, 2
- [13] Zhengyang Geng, Mingyang Deng, Xingjian Bai, J Zico Kolter, and Kaiming He. Mean flows for one-step generative modeling. *arXiv preprint arXiv:2505.13447*, 2025. 1, 2, 4, 7, 8
- [14] Zhengyang Geng, Ashwini Pokle, Weijian Luo, Justin Lin, and J Zico Kolter. Consistency models made easy. In *The Thirteenth International Conference on Learning Representations*, 2025. 2, 5, 8
- [15] Pengsheng Guo and Alex Schwing. Variational rectified flow matching. In *Forty-second International Conference on Machine Learning*, 2025. 1, 2, 4, 5, 8
- [16] Martin Heusel, Hubert Ramsauer, Thomas Unterthiner, Bernhard Nessler, and Sepp Hochreiter. Gans trained by a two time-scale update rule converge to a local nash equilibrium. *Advances in neural information processing systems*, 30, 2017. 6
- [17] Emiel Hoogeboom, Jonathan Heek, and Tim Salimans. simple diffusion: End-to-end diffusion for high resolution images. In *International Conference on Machine Learning*, pages 13213–13232. PMLR, 2023. 1
- [18] Zheyuan Hu, Chieh-Hsin Lai, Yuki Mitsufuji, and Stefano Ermon. Cmt: Mid-training for efficient learning of consistency, mean flow, and flow map models. *arXiv preprint arXiv:2509.24526*, 2025. 2
- [19] Yingrui Ji, Xi Xiao, Gaofei Chen, Hao Xu, Chenrui Ma, Li-jing Zhu, Aokun Liang, and Jiansheng Chen. Cibr: Cross-modal information bottleneck regularization for robust clip generalization. In *International Conference on Artificial Neural Networks*, pages 247–259. Springer, 2025. 2
- [20] Yang Jin, Zhicheng Sun, Ningyuan Li, Kun Xu, Kun Xu, Hao Jiang, Nan Zhuang, Quzhe Huang, Yang Song, Yadong MU, and Zhouchen Lin. Pyramidal flow matching for efficient video generative modeling. In *The Thirteenth International Conference on Learning Representations*, 2025. 6
- [21] Dongjun Kim, Chieh-Hsin Lai, Wei-Hsiang Liao, Naoki Murata, Yuhta Takida, Toshimitsu Uesaka, Yutong He, Yuki Mitsufuji, and Stefano Ermon. Consistency trajectory models: Learning probability flow ODE trajectory of diffusion. In *The Twelfth International Conference on Learning Representations*, 2024. 1, 2
- [22] Diederik P Kingma and Max Welling. Auto-encoding variational bayes. *arXiv preprint arXiv:1312.6114*, 2013. 1
- [23] Leon Klein, Andreas Krämer, and Frank Noé. Equivariant flow matching. *Advances in Neural Information Processing Systems*, 36:59886–59910, 2023. 1
- [24] Nikita Kornilov, Petr Mokrov, Alexander Gasnikov, and Aleksandr Korotin. Optimal flow matching: Learning straight trajectories in just one step. *Advances in Neural Information Processing Systems*, 37:104180–104204, 2024. 2

[25] Alex Krizhevsky, Geoffrey Hinton, et al. Learning multiple layers of features from tiny images. 2009. 5

[26] Alex Krizhevsky, Ilya Sutskever, and Geoffrey E Hinton. Imagenet classification with deep convolutional neural networks. *Advances in neural information processing systems*, 25, 2012. 6

[27] Sangyun Lee, Zinan Lin, and Giulia Fanti. Improving the training of rectified flows. *Advances in neural information processing systems*, 37:63082–63109, 2024. 1, 2

[28] Yaron Lipman, Ricky T. Q. Chen, Heli Ben-Hamu, Maximilian Nickel, and Matthew Le. Flow matching for generative modeling. In *The Eleventh International Conference on Learning Representations*, 2023. 1, 3, 4, 8

[29] Yaron Lipman, Marton Havasi, Peter Holderith, Neta Shaul, Matt Le, Brian Karrer, Ricky TQ Chen, David Lopez-Paz, Heli Ben-Hamu, and Itai Gat. Flow matching guide and code. *arXiv preprint arXiv:2412.06264*, 2024. 1, 3

[30] Xingchao Liu, Chengyue Gong, and qiang liu. Flow straight and fast: Learning to generate and transfer data with rectified flow. In *The Eleventh International Conference on Learning Representations*, 2023. 1, 2, 3, 8

[31] Cheng Lu and Yang Song. Simplifying, stabilizing and scaling continuous-time consistency models. In *The Thirteenth International Conference on Learning Representations*, 2025. 2, 8

[32] Chenrui Ma, Xi Xiao, Tianyang Wang, and Yanning Shen. Beyond editing pairs: Fine-grained instructional image editing via multi-scale learnable regions. *arXiv preprint arXiv:2505.19352*, 2025. 6

[33] Chenrui Ma, Xi Xiao, Tianyang Wang, Xiao Wang, and Yanning Shen. CAD-VAE: Leveraging correlation-aware latents for comprehensive fair disentanglement. In *The Fortieth AAAI Conference on Artificial Intelligence*, 2025. 1

[34] Chenrui Ma, Xi Xiao, Tianyang Wang, Xiao Wang, and Yanning Shen. Stochastic interpolants via conditional dependent coupling. *arXiv preprint arXiv:2509.23122*, 2025. 1

[35] Nanye Ma, Mark Goldstein, Michael S Albergo, Nicholas M Boffi, Eric Vanden-Eijnden, and Saining Xie. Sit: Exploring flow and diffusion-based generative models with scalable interpolant transformers. In *European Conference on Computer Vision*, pages 23–40. Springer, 2024. 6, 7, 8

[36] Kangfu Mei, Mauricio Delbracio, Hossein Talebi, Zhengzhong Tu, Vishal M Patel, and Peyman Milanfar. Codi: Conditional diffusion distillation for higher-fidelity and faster image generation. In *Proceedings of the IEEE/CVF Conference on Computer Vision and Pattern Recognition*, pages 9048–9058, 2024. 2

[37] James R Norris. *Markov chains*. Number 2. Cambridge university press, 1998. 4

[38] Aram-Alexandre Pooladian, Heli Ben-Hamu, Carles Domingo-Enrich, Brandon Amos, Yaron Lipman, and Ricky TQ Chen. Multisample flow matching: Straightening flows with minibatch couplings. In *International Conference on Machine Learning*, pages 28100–28127. PMLR, 2023. 1

[39] Amirmojtaba Sabour, Sanja Fidler, and Karsten Kreis. Align your flow: Scaling continuous-time flow map distillation. *arXiv preprint arXiv:2506.14603*, 2025. 1

[40] Tim Salimans and Jonathan Ho. Progressive distillation for fast sampling of diffusion models. In *International Conference on Learning Representations*, 2022. 1, 2

[41] Gianluigi Silvestri, Luca Ambrogioni, Chieh-Hsin Lai, Yuhta Takida, and Yuki Mitsufuji. VCT: Training consistency models with variational noise coupling. In *Forty-second International Conference on Machine Learning*, 2025. 1

[42] Yang Song and Prafulla Dhariwal. Improved techniques for training consistency models. In *The Twelfth International Conference on Learning Representations*, 2024. 1, 2, 7, 8

[43] Yang Song, Prafulla Dhariwal, Mark Chen, and Ilya Sutskever. Consistency models. In *Proceedings of the 40th International Conference on Machine Learning*, pages 32211–32252, 2023. 1, 2, 8

[44] Alexander Tong, Kilian Fatras, Nikolay Malkin, Guillaume Huguet, Yanlei Zhang, Jarrid Rector-Brooks, Guy Wolf, and Yoshua Bengio. Improving and generalizing flow-based generative models with minibatch optimal transport. *arXiv preprint arXiv:2302.00482*, 2023. 1

[45] Cédric Villani et al. *Optimal transport: old and new*. Springer, 2008. 1

[46] Ziyu Wan, Despoina Paschalidou, Ian Huang, Hongyu Liu, Bokui Shen, Xiaoyu Xiang, Jing Liao, and Leonidas Guibas. Cad: Photorealistic 3d generation via adversarial distillation. In *Proceedings of the IEEE/CVF Conference on Computer Vision and Pattern Recognition*, pages 10194–10207, 2024. 2

[47] Fu-Yun Wang, Ling Yang, Zhaoyang Huang, Mengdi Wang, and Hongsheng Li. Rectified diffusion: Straightness is not your need in rectified flow. *arXiv preprint arXiv:2410.07303*, 2024. 1, 2

[48] Tianwei Yin, Michaël Gharbi, Taesung Park, Richard Zhang, Eli Shechtman, Fredo Durand, and Bill Freeman. Improved distribution matching distillation for fast image synthesis. *Advances in neural information processing systems*, 37:47455–47487, 2024. 2

[49] Tianwei Yin, Michaël Gharbi, Richard Zhang, Eli Shechtman, Fredo Durand, William T Freeman, and Taesung Park. One-step diffusion with distribution matching distillation. In *Proceedings of the IEEE/CVF conference on computer vision and pattern recognition*, pages 6613–6623, 2024. 2

[50] Haochen You, Baojing Liu, and Hongyang He. Modular meanflow: Towards stable and scalable one-step generative modeling. *arXiv preprint arXiv:2508.17426*, 2025. 2

[51] Hui Zhang, Dexiang Hong, Yitong Wang, Jie Shao, Xinglong Wu, Zuxuan Wu, and Yu-Gang Jiang. Creatilayout: Siamese multimodal diffusion transformer for creative layout-to-image generation. In *Proceedings of the IEEE/CVF International Conference on Computer Vision*, pages 18487–18497, 2025. 6

[52] Huijie Zhang, Aliaksandr Siarohin, Willi Menapace, Michael Vasilkovsky, Sergey Tulyakov, Qing Qu, and Ivan Skorokhodov. Alphaflow: Understanding and improving meanflow models. *arXiv preprint arXiv:2510.20771*, 2025. 1, 2

- [53] Yichi Zhang, Yici Yan, Alex Schwing, and Zhizhen Zhao. Hierarchical rectified flow matching with mini-batch couplings. *arXiv preprint arXiv:2507.13350*, 2025. [1](#), [2](#)
- [54] Yichi Zhang, Yici Yan, Alex Schwing, and Zhizhen Zhao. Towards hierarchical rectified flow. In *The Thirteenth International Conference on Learning Representations*, 2025. [1](#), [2](#)
- [55] Linqi Zhou, Stefano Ermon, and Jiaming Song. Inductive moment matching. In *Forty-second International Conference on Machine Learning*, 2025. [2](#), [8](#)

Learning Straight Flows: Variational Flow Matching for Efficient Generation

Supplementary Material

7. Proofs for Straight, Non-Intersecting Interpolations

This appendix develops, in a self-contained way, the analytical objects and proofs underlying our method. We introduce a *straight, non-intersecting interpolation* Z that is *compatible* with the linear interpolation induced by a given coupling X , and we establish: (i) preservation of time marginals, (ii) reduction of convex transport costs, and (iii) equivalent characterizations of straight (non-intersecting) couplings.

Notation. For a random process $X = \{X_t\}_{t \in [0,1]}$, write $\text{Law}(X_t)$ for its marginal law at time t , and $\mathbb{E}[\cdot]$ for expectation. For a coupling (X_0, X_1) we denote $\Delta^X := X_1 - X_0$ and the linear interpolant $X_t = (1-t)X_0 + tX_1$. Conditional expectations such as $\mathbb{E}[\Delta^X | X_t = x]$ are understood whenever they exist.

7.1. Preliminaries

Definition 5 (Coupling, linear interpolation, and conditional velocity). Let (X_0, X_1) be any coupling on \mathbb{R}^d with joint density $\rho(x_0, x_1) = \rho_0(x_0) \rho_1(x_1)$. Define the linear interpolation

$$X_t = (1-t)X_0 + tX_1, \quad t \in [0, 1]$$

$$\Delta^X = v^X(X_t, t | (X_0, X_1)) = X_1 - X_0.$$

The *marginal velocity* associated with X is

$$v^X(x, t) = \mathbb{E}[\Delta^X | X_t = x], \quad (x, t) \in \mathbb{R}^d \times [0, 1]$$

$$= \int \Delta^X \cdot p(X_0, X_1 | X_t = x) d(X_0, X_1).$$

When $x \notin \text{supp}(X_t)$, we set $v^X(x, t) = 0$. All statements below compare v^X only on sets where it is evaluated against a marginal law: $\text{Law}(X_t)$.

Definition 6 (Rectifiability of X). We say that X is *rectifiable* if $v^X(\cdot, t)$ is locally bounded for each t and the continuity equation

$$\partial_t \pi_t + \nabla \cdot (v^X(\cdot, t) \pi_t) = 0, \quad \pi_{t=0} = \text{Law}(X_0),$$

admits a unique solution $\{\pi_t\}_{t \in [0,1]}$. Equivalently, the ordinary differential equation $\dot{X}_t = v^X(X_t, t)$ admits a unique flow of characteristics.

Definition 7 (Non-intersection functional). For any coupling (X_0, X_1) with linear interpolant X_t , define

$$V((X_0, X_1)) := \int_0^1 \mathbb{E}[\|\Delta^X - \mathbb{E}[\Delta^X | X_t]\|^2] dt.$$

Lemma 6 (Non-intersection if and only if zero conditional variance). For a coupling (X_0, X_1) with linear interpolation X_t , the following are equivalent:

1. For two independent identically distributed couplings (X_0, X_1) and (X'_0, X'_1) ,

$$\exists t \in (0, 1) : (1-t)X_0 + tX_1 = (1-t)X'_0 + tX'_1$$

$$\mathbb{P}[(X_0, X_1) \neq (X'_0, X'_1)] = 0.$$

2. $V((X_0, X_1)) = 0$; equivalently $\Delta^X = \mathbb{E}[\Delta^X | X_t]$ for $t \in [0, 1]$.

Proof. (1) \Rightarrow (2) : Non-intersection implies that the slope Δ^X is a measurable function of (X_t, t) , hence $\text{Var}(\Delta^X | X_t) = 0$; integrating over t gives $V = 0$. (2) \Rightarrow (1) : If $\Delta^X = \mathbb{E}[\Delta^X | X_t]$, then the slope through any X_t is unique, two distinct lines cannot share a point at the same time unless they coincide. \square

7.2. The straight interpolation Z compatible with X

Definition 8 (Straight interpolation compatible with X). A process $Z = \{Z_t\}_{t \in [0,1]}$ on the same probability space as X is called a *straight interpolants* compatible with Flow Matching trajectories X if the following hold:

(Z1) **Linear paths.** There exist random endpoints (Z_0, Z_1) with $Z_t = (1-t)Z_0 + tZ_1$ and $\Delta^Z := Z_1 - Z_0$.

(Z2) **Non-intersection.** $V((Z_0, Z_1)) = 0$. Equivalently, $\Delta^Z = \mathbb{E}[\Delta^Z | Z_t]$ for $t \in [0, 1]$.

(Z3) **Velocity-field matching.** With $\mu_t = \text{Law}(Z_t)$, for $x \sim \mu_t$ and $t \in [0, 1]$,

$$v^Z(x, t) := \mathbb{E}[\Delta^Z | Z_t = x] = v^X(x, t).$$

(Z4) **Initialization.** $Z_0 = X_0$.

Remark 7 (Immediate consequences). From (Z2), $v^Z(Z_t, t) = \Delta^Z$, hence

$$Z_1 - Z_0 = \int_0^1 v^Z(Z_t, t) dt.$$

By (Z3), $v^Z = v^X$ at $x \sim \mu_t$, so we also have

$$\Delta^Z = \int_0^1 v^X(Z_t, t) dt.$$

7.3. Main results

Theorem 8 (Marginal preservation). Assume X is rectifiable and Z satisfies Definition 8. Then $\text{Law}(Z_t) = \text{Law}(X_t)$ for all $t \in [0, 1]$.

Proof. Let $h : \mathbb{R}^d \rightarrow \mathbb{R}$ be any compactly supported continuously differentiable test function. Using (Z1) and (Z2),

$$\begin{aligned}\frac{d}{dt} \mathbb{E}[h(Z_t)] &= \mathbb{E}[\nabla h(Z_t)^\top \dot{Z}_t] = \mathbb{E}[\nabla h(Z_t)^\top \Delta^Z] \\ &= \mathbb{E}[\nabla h(Z_t)^\top v^Z(Z_t, t)].\end{aligned}$$

By (Z3), $v^Z(\cdot, t) = v^X(\cdot, t)$ for μ_t , therefore

$$\frac{d}{dt} \mathbb{E}[h(Z_t)] = \mathbb{E}[\nabla h(Z_t)^\top v^X(Z_t, t)].$$

This shows that $\mu_t = \text{Law}(Z_t)$ solves the continuity equation $\partial_t \mu_t + \nabla \cdot (v^X(\cdot, t) \mu_t) = 0$ with $\mu_0 = \text{Law}(Z_0) = \text{Law}(X_0)$ by (Z4). By rectifiability of X , the solution is unique and equals $\pi_t = \text{Law}(X_t)$. Hence $\mu_t = \pi_t$ for all $t \in [0, 1]$. \square

Theorem 9 (Convex transport-cost reduction). *Under the assumptions of Theorem 8, for any convex $c : \mathbb{R}^d \rightarrow \mathbb{R}$,*

$$\mathbb{E}[c(Z_1 - Z_0)] \leq \mathbb{E}[c(X_1 - X_0)].$$

If c is strictly convex, equality holds if and only if $V((X_0, X_1)) = 0$.

Proof. From (Z2),

$$Z_1 - Z_0 = \int_0^1 v^Z(Z_t, t) dt.$$

By Jensen's inequality in time,

$$\mathbb{E}[c(Z_1 - Z_0)] \leq \int_0^1 \mathbb{E}[c(v^Z(Z_t, t))] dt.$$

Using (Z3) and Theorem 8,

$$\begin{aligned}\int_0^1 \mathbb{E}[c(v^Z(Z_t, t))] dt &= \int_0^1 \mathbb{E}[c(v^X(X_t, t))] dt \\ &= \int_0^1 \mathbb{E}[c(\mathbb{E}[\Delta^X | X_t])] dt.\end{aligned}$$

A conditional Jensen inequality (conditioning on X_t) yields

$$\mathbb{E}[c(\mathbb{E}[\Delta^X | X_t])] \leq \mathbb{E}[\mathbb{E}[c(\Delta^X) | X_t]] = \mathbb{E}[c(\Delta^X)].$$

Combining gives the inequality. If c is strictly convex, equality forces tightness of the conditional Jensen step, hence $\Delta^X = \mathbb{E}[\Delta^X | X_t]$, which by Lemma 6 is $V((X_0, X_1)) = 0$. \square

Theorem 10 (Equivalent characterizations of straight interpolants). *Assume X is rectifiable and Z satisfies Definition 8. The following are equivalent: when they hold, we say X yielded from couplings (X_0, X_1) are straight interpolants, which coincide with Z .*

- (i) **Tight convex cost.** There exists a strictly convex c with $\mathbb{E}[c(Z_1 - Z_0)] = \mathbb{E}[c(X_1 - X_0)]$.
- (ii) **Endpoint coincidence.** $(Z_0, Z_1) = (X_0, X_1)$.
- (iii) **Pathwise equality.** $Z_t = X_t$ for all $t \in [0, 1]$.
- (iv) **Non-intersection for X .** $V((X_0, X_1)) = 0$.

Proof. 1. (iii) \implies (ii) is immediate.

2. (ii) \implies (i) turns the inequality of Theorem 9 into equality.

3. (i) \implies (iv): In Theorem 9 with strictly convex c , equality forces tightness of the conditional Jensen step; hence $\Delta^X = \mathbb{E}[\Delta^X | X_t]$ for $t \in [0, 1]$, which is $V((X_0, X_1)) = 0$ by Lemma 6.

4. (iv) \implies (iii): If $V((X_0, X_1)) = 0$, then for $t \in [0, 1]$, $\dot{X}_t = \Delta^X = v^X(X_t, t)$. For Z , (Z2)–(Z3) give $\dot{Z}_t = \Delta^Z = v^Z(Z_t, t) = v^X(Z_t, t)$. Hence both X and Z solve $\dot{Y}_t = v^X(Y_t, t)$ with the same initial value $Y_0 = X_0 = Z_0$ by (Z4). Uniqueness of rectifiability in Definition 6 yields $Z \equiv X$. \square

Corollary 11 (One-step generation). *If any, and therefore all, of the items in Theorem 10 hold, then along each path $v^X(X_t, t) \equiv \Delta^X$ is constant in t and the ordinary differential equation $\dot{y}_t = v^X(y_t, t)$ integrates in one step:*

$$X_1 = X_0 + \int_0^1 v^X(X_t, t) dt = X_0 + \Delta^X.$$

7.4. Equivalence with vanishing time derivative

Definition 9 (Time derivative). For a differentiable vector field $v : \mathbb{R}^d \times [0, 1] \rightarrow \mathbb{R}^d$, the time derivative along its characteristics is

$$\begin{aligned}\frac{d}{dt} v(x, t) &= D_t v(x, t) := \frac{\partial v}{\partial t} \frac{dt}{dt} + \frac{\partial v}{\partial x} \frac{dx}{dt} \\ &= \frac{\partial}{\partial t} v(x, t) + (\nabla_x v(x, t)) v(x, t)\end{aligned}$$

Theorem 12 (Straightness if and only if vanishing time derivative along X). *Assume X is rectifiable and Z satisfies Definition 8. Assume moreover that v^X is continuously differentiable in (x, t) . Then $V((X_0, X_1)) = 0$, if and only if $D_t v^X(X_t, t) = 0$, for $t \in [0, 1]$.*

Proof. \Rightarrow : If $V = 0$, Theorem 10 gives $Z \equiv X$ and $v^X(X_t, t) = \Delta^X$, which is constant in t along each path. The chain rule implies $D_t v^X(X_t, t) = \partial_t v^X(X_t, t) + \nabla v^X(X_t, t) \dot{X}_t = 0$.

\Leftarrow : If $D_t v^X(X_t, t) = 0$ for $t \in [0, 1]$, then $v^X(X_t, t)$ is constant in t along each path. With $Z_0 = X_0$, the solution has the linear form $X_t = (1-t)X_0 + tX_1$ and distinct trajectories cannot intersect because the ordinary differential equation with a well-posed vector field has unique solutions. By Theorem 8, $\text{Law}(Z_t) = \text{Law}(X_t)$ for all t . Applying Theorem 10 then yields $V((X_0, X_1)) = 0$. \square